Hammerstein–Wiener Modeling of a Magneto-Rheological Dampers Considering the Magnetization Dynamics

Gianluca Savaia[a], Giulio Panzani[a,*], Matteo Corno[a], Jacopo Cecconi[b], Sergio M. Savaresi[a]

[a]*Dipartimento di Elettronica, Informazione e Bioingegneria, Politecnico di Milano, Italy*
[b]*Automobili Lamborghini s.p.a, Italy*

Abstract

Magneto-rheological dampers are an effective technology to control the damping coefficient of a semi-active suspension. Most of the contributions in literature propose damper models to be used in simulation, or as damping force virtual sensors in control applications. Typically, phenomenological models or complex black-box approaches, relying on Neural Networks, are employed. In this work, we propose a semi-active MR model based on a Hammerstein–Wiener scheme, meant not only for force estimation but also – in a more genuinely control-oriented perspective – to be proactively used in the suspension controller design. Despite being a black-box model, each component is shown to serve for the characterization of a specific feature of the MR damper, and its identification is done thanks to an *ad hoc* design of experiments. In particular, the Wiener part of the model is shown to be essential for the proper modelling of the magnetization dynamics of the magneto-rheological fluid, which usually is a neglected aspect in control-oriented models. The proposed scheme is validated on a testbench using realistic road solicitations.

DOI: 10.1016/j.conengprac.2021.104829

Keywords: magneto-rheological damper, control-oriented model, Hammerstein–Wiener model, design of experiments.

1. Introduction

Semi-active dampers, *i.e.* dampers that are capable of changing their damping coefficients in a matter of milliseconds, provide a good trade-off between control authority, packaging, power consumption and fail safe operability. For these reasons, they are the preferred approach to electronic suspension control.

Several technologies exist to achieve semi-active damping: Electro Hydraulic (EH), Electro-rheological (ER) and Magneto-rheological (MR) are the most common. In MR (and ER) dampers, a fluid changes its viscosity when subject to a magnetic field [1] (or to an electric field). Due to the lack of moving valves, ER and MR dampers allow (all other factors being equal) for a higher frequency modulation of the damping coefficient with respect to EH. Moreover, MR and ER can achieve higher forces at low stroke speed. Due to their similarities there is no specific distinction in modelling MR and ER dampers, see *e.g.* [2] and owing to the fact the it is easier to generate a strong magnetic field than an electric field using automotive grade components, MR dampers are enjoining more popularity among Original Equipment Manufacturers and also in the scientific literature.

MR dampers have been extensively investigated by

*Corresponding author: giulio.panzani@polimi.it

many researchers in the past two decades and different modelling approaches have been proposed. One can classify these approaches among two orthogonal axes: type of models and objectives.

There exist three types of model: Physical, Phenomenological and Black-box models.

Physical models [3, 4, 5] are first-principle models that solve complex fluid dynamics equations. They have the potential of being very accurate at a cost of being extremely complex to simulate and expensive to calibrate.

Phenomenological models describe the damper as a connection of elemental mechanical elements (*e.g.* springs and viscous dashpots) so to match the characteristics of the MR damper. References [6, 7, 8] provide a comprehensive overview of this area. Different works put forward different methods to describe the MR damper nonlinearities. The most popular approaches are the Bingham [9], Bouc-Wen [9, 10], Dahl [11] and LuGre [12] models. Note that, in the literature, the force–current dependency is often not investigated in detail: a typical approach consists in interpolating the parameters of different constant current models, as in [13, 14, 15] or to interpolate the output force of each model with respect to the current [16].

Black-box modelling describes the input – output (damper speed, current – damping force) relationship using a mathematical representation which has no direct correspondence to any physical phenomena occurring in the damper. Polynomial models [17], fuzzy models [18, 19], NARX models [20] and models based on neural networks [21, 22, 23, 24, 25] are examples of this approach.

The second classification axis deals with the objective of the model. We identify three scopes: Simulation-oriented models, actuator-oriented control models and vehicle-oriented control models.

Simulation-oriented models are engineered for control strategy or design validation [26, 27, 28]. All the above modelling approaches find their place in this context and usually the higher the model accuracy, the better, even at the cost of complexity.

Actuator-oriented control models provide tools to design the low level actuator control. The objective of the low level control is force tracking *i.e.* to determine the damper current that yields a desired force. One common approach is to invert the MR damper model. In [29, 30], the inversion is based on the Bingham model (which also neglects the speed-to-force dynamics). In [31], the authors employ the Bouc-Wen model to implement another static approach, neglecting the current to force dynamics. Few authors explicitly consider dynamics aspects in the damper inversion, at most considering the hysteresis; see for example [32, 33, 34, 35].

Two other approaches are available to avoid neglecting the dynamics. One is based on a direct identification of the inverse damper model, usually using Neural-Networks, see [36, 21, 37, 24]. The second solution implements the inversion through a simulated closed-loop [38, 39, 40]: the controlled plant is represented by the MR damper model and a feedback controller operates on a "virtual" current in order to track the reference force. The main advantage of this approach is that it can potentially employ any time of model, even very complex and accurate ones. The main disadvantage is related to the presence of the closed-loop; its design has to meet stability and performance criteria. As a matter of fact, none of the mentioned papers explicitly addresses these closed-loop issues, mainly due to the complex analytical nature of the available damper models.

Vehicle-oriented control models are useful to directly design vehicle dynamics controllers. Several authors proposed control strategies tailored to MR dampers [41]. In most works, the MR damper description is approximated, so to be embedded in the control analysis and design. In [42], a Takagi-Sugeno fuzzy approximation of the vehicle and MR damper is done. Linear or linearized damper descriptions are used for the control design or analysis in [43]. Alternatively, robust control techniques [44, 30, 45] are used to deal with the damper model approximation. We found few works that address the design of vehicle control strategies without any important model simplification. In [46], the authors use a nonparametric model [47] to prove stability with the circle criterion. In [48], the Bouc-Wen MR damper model is considered and the control stability relies on a Lyapunov approach. In [49, 50], a mixed phenomenological – black-box model is cast into an LPV framework for the design of the vehicle level semi-active controller.

LPV techniques are also used in [51, 52] for the design of an observer which allows the damper faults detection.

In simulation-oriented models, the complexity of the model only affects simulation time. In that context, we thus refer to complexity only in terms of computational load. In control models, as discussed, complexity mainly involves the mathematical structure of the model. The more mathematically treatable the model is, the easier is to design controllers and estimators with strong formal guarantees. The ideal control model should be able to effectively and as simply as possible capture all important damper dynamics.

In this paper, we propose a control oriented model according to the above considerations. We show that a Hammerstein-Wiener (HW) model can, within a unified framework, capture all the main dynamic characteristics of the damper: current, stroke speed and temperature effects. Hammerstein-Wiener (HW) models define a relatively simple, yet powerful model class, for which many calibration and control analysis tools are available [53, 54, 55, 56]. They are thus particularly suited for direct use in the design of feedback control systems.

Despite these advantages, Hammerstein-Wiener models are not common in the MR damping literature. The few works that present Hammerstein-Wiener models focus on specific aspects of the damper dynamics: in [57, 58], the authors employ a Hammerstein model to model a passive MR damper, thus neglecting the current dynamics and the temperature effect. In [59, 60], a Wiener model considers the effect of the current, but as static term. In [47], the authors propose a Hammerstein-like approach that accounts for the current dynamics by introducing a nonlinear current dependency of the model coefficients. This approach, while accurate, increases the mathematical complexity of the model. Other Hammerstein inspired approaches that use a parallel connection between the linear dynamics and the nonlinear static block are [61, 33, 21, 35]. Also in this case, the current dependency is described with a static model neglecting the magnetization dynamics

Based on the above discussion, our contributions can be summarized as:

- We derive, identify and validate an HW model that considers stroke speed to force and current to force dynamics, and the temperature effect. While all these phenomena have been studied and considered in the literature, to the best of our knowledge, no previously published work offers a unified HW model dealing with all the phenomena.

- We describe a specific HW experimental procedure for the identification of each model part. This improves reusabilty and simplify model maintenance.

- We provide a quantitative analysis of the role each element of the model plays in describing the overall MR damper behaviour. This proves the flexibility and physical interpretability of our model.

- We provide a quantitative evaluation of the accuracy of our model against a Neural-Network model. This helps to assess the modelling performance in absolute terms.

The remainder of this paper is as follows. In Section 2, the experimental setup used for analysing the MR damper phenomena is presented. The model identification of the Hammerstein-Wiener scheme is discussed in Section 3 along with the design of experiments and results. The model is validated with a realistic road excitation in Section 4. The paper is ended by some concluding remarks.

2. Experimental Setup

The damper tested in this work is a standard automotive component, which features an overall stroke of 60mm.

The experiments used for the identification and the validation of the damper model have been performed on an servo-hydraulic test bench capable of replicating a desired stroke profile, ranging from standard triangular or sinusoidal waves to custom measured road profiles. The bench employs high precision encoders and velocity preservation compensators to track a

reference displacement profile with very low distortion. Furthermore, the damper is located in a climatic chamber where the ambient temperature can be controlled between -30 ℃ and +100 ℃. The experimental setup is shown in Figure 1.

The testing machine has an upper and lower head with grippers which the damper is locked to. The lower head is the movable end and is operated by a hydraulic actuator which follows the reference displacement profile, whereas in the upper head there is a load cell which can measure the actual force exerted by the damper. A thermocouple has been also inserted into the damper oil chamber in order to measure the actual internal temperature of the MR fluid; it can measure temperatures in the range between -50 and +200°C, with a response time of 200ms and a resolution of 0.2 °C. When not specified, the temperature values refer to the internal MR damper fluid ones, measured by the thermocouple.

An off-the-shelf, commercial Electronic Control Unit implements the closed-loop control of the current so that our interface with the damper is a desired current. The current control has a bandwidth of 200 Hz. We remark that the model discussed in the remainder of the paper is independent from the current closed-loop control performances as it employs the measured current as one input variable.

All the relevant measures – damper force, stroke, current and internal temperature – are sampled at 5kHz.

3. Modeling and Identification

In this section, the main phenomena characterizing a MR damper are investigated through an *ad hoc* design of experiments; for thorough surveys on the characterization of MR dampers see [62, 63].

The main ingredients that contribute to the MR damper force generation are:

- *Damping Characteristics*, a static relationship between stroke speed and damping force;
- *Hysteretic Behavior*, a dynamic relationship between stroke speed and damping force;
- *Magnetization Dynamics*, a transient occurring when the control current is changed;
- *Temperature Effect*, affecting the maximum damping force which can be exerted by the damper.

The control-oriented model proposed in this contribution is based on the Hammerstein-Wiener scheme depicted in Figure 2, and it is meant to capture all the mentioned phenomena: the static nonlinear block C is in charge of modelling the *Damping Characteristics* and the effects due to temperature; the Hammerstein block $H(s)$ captures the dynamic relationship due to the stroke elongation rate; eventually, the Wiener block $M(s)$ models the magnetization dynamics. The positions of the dynamic blocks $H(s)$ and $M(s)$ (*i.e.* Hammerstein and Wiener) are chosen according to an intuition from the physics of the device: when the MR fluid is exposed to the magnetic field generated by current in the solenoid, there exists a transient period before the damping force effectively develops; similarly, the Hammerstein block represents the memory of the device which causes the hysteretic behaviour observed in the damping force, and it is therefore placed at the end of the series.

In the following, the contribution of each block is carefully elaborated and the model is identified using *ad hoc* experiments aimed at emphasizing the phenomenon which they intend to characterize.

3.1. Damping Characteristics

The nonlinear static block of the Hammerstein-Wiener scheme describes the main force contribution in a MR damper, being the friction force generated when the fluid flows into the orifices in the piston. Such force depends on the stroke speed and the fluid viscosity, which can be adjusted thanks to the input current. The resulting relationship is known as damping characteristic of the component.

In order to collect the experimental data to identify this nonlinear block, the piston is moved along the whole stroke length at different constant speeds, as shown in Figure 3. For each speed value, the corresponding force is collected, and the resulting pair is reported in the force–speed phase plane. The resulting damper characteristic, for a constant current

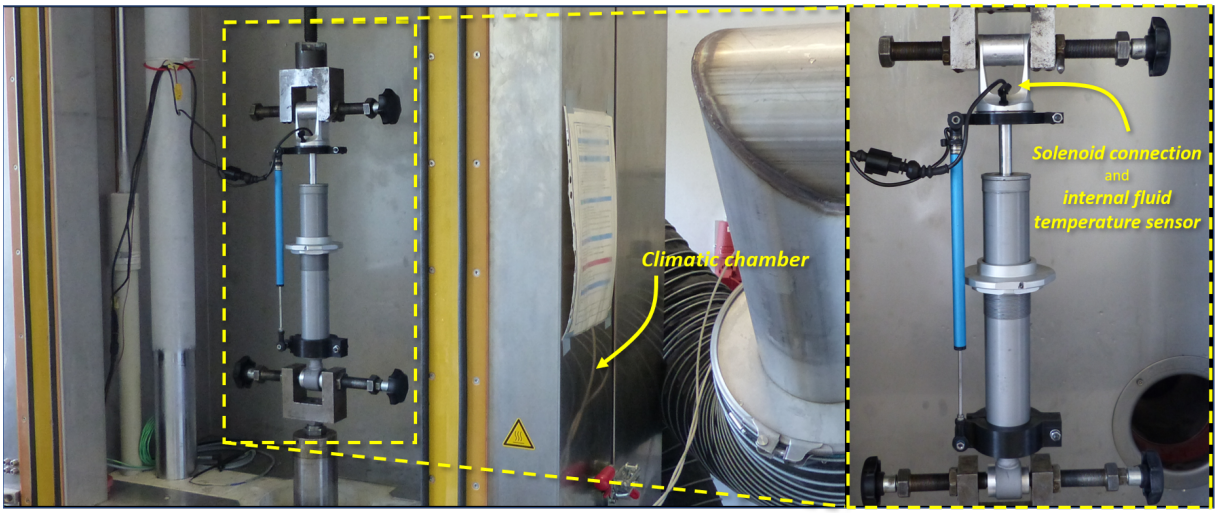

Figure 1: The test bench used for the damper experiments.

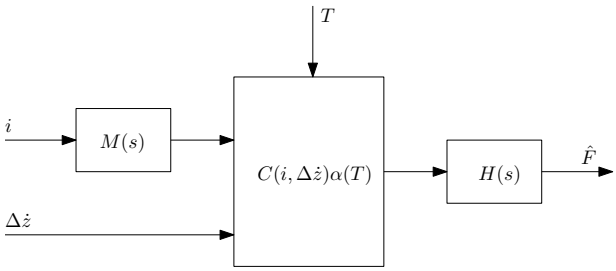

Figure 2: The Hammerstein-Wiener scheme used to model the MR damper.

value, is shown in Figure 4: it exhibits the typical pre-yield region, characterized by a high slope, and post-yield region which flattens out beyond 100 mm/s. The symmetry of the damping characteristics with respect to the compression and extension phase is noteworthy, as it is not usual in other damper technologies. By replicating the same experiment using different current values, it is possible to extract the whole controllability region of the damper, shown in Figure 5. The shape of the curve is similar for each current and its main effect is the increase of the maximum damping force, due to the shift the post-yield region to higher stroke speed values.

The experimental damping characteristics are modelled by the nonlinear static relationship

$$\hat{F}_c = C(i, \Delta\dot{z}) \tag{1}$$

where C indicates the *damping curve* relative to a current i along the stroke speed profile $\Delta\dot{z}$. The surface C can be analytically described by different operators (*e.g.* linear piecewise function, neural network with logistic activation, polynomials, *etc.*); each representation is equally valid as long as it minimizes the estimation error with respect to the experimental points on the force-speed plane. Here, a linear piecewise function:

$$C(i, \Delta\dot{z}) = \\ = \begin{cases} c_{post} \cdot (\Delta\dot{z} - \Delta_0) + c_{pre}\Delta_0 & \text{for} \quad \Delta\dot{z} > \Delta_0 \\ c_{pre} \cdot \Delta\dot{z} & \text{for} \quad -\Delta_0 \leq \Delta\dot{z} \leq \Delta_0 \\ c_{post} \cdot (\Delta\dot{z} - \Delta_0) - c_{pre}\Delta_0 & \text{for} \quad \Delta\dot{z} < -\Delta_0 \end{cases} \tag{2}$$

has been used. The symmetric damper behaviour with respect to positive and negative stroke velocities allows for a reduced number of parameters, namely c_{pre}, c_{post} and Δ_0. The effect of the current on the damper force can be modelled with an affine function of the Δ_0 parameter with respect to the input current $\Delta_0 = \Delta_0(i) = a \cdot i + b$. Figure 5 shows the comparison

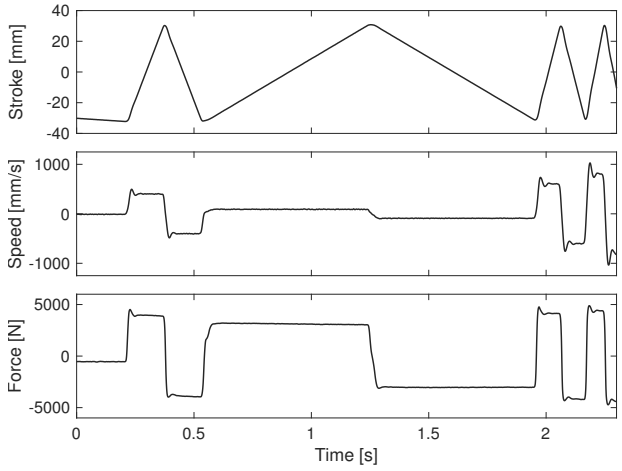

Figure 3: Constant stroke speed experiments for the identification of the damping characteristic.

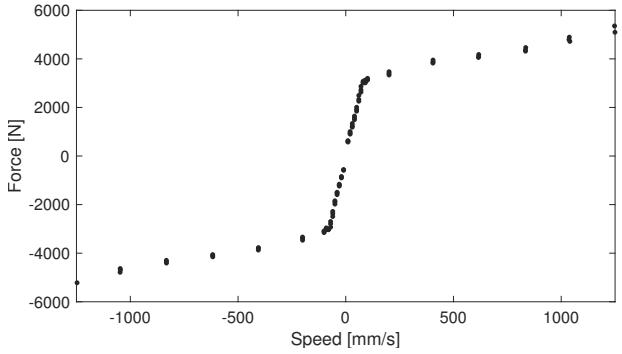

Figure 4: Experimental force–speed nonlinear relationship.

between the resulting model and the experimental data.

Due to their limited duration, the constant stroke speed tests do not affect the internal fluid temperature whose influence has been so far neglected. Nevertheless, scientific literature well documents how this parameter significantly affects the MR fluid viscosity [64]: the higher the temperature, the less viscous the fluid and, consequently, the less force exerted by the damper. In automotive applications the typical operating temperature ranges from -30 °C to +140 °C. Hence, this variability needs to be accounted in the damper model.

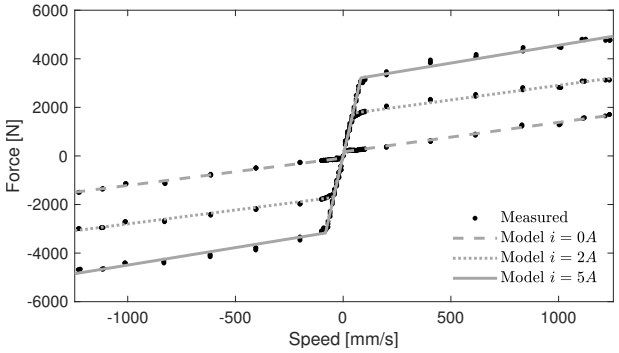

Figure 5: Comparison between the force–speed experimental maps and the corresponding piecewise affine model, for different current values.

In order to investigate the temperature effect, the constant frequency sine wave test shown in Figure 6 has been performed. Due to the mechanical dissipated power, the damper temperature (visible in the lower plot) increases during the test, making possible to experimentally analyse its effect on the resulting damping force. Thanks to the availability of the climatic chamber, different ambient temperatures were set; letting the damper rest in the climatic chamber allowed us to start the test with different damper fluid internal temperatures. The choice of the sine wave frequency is important for the design of the experiment, as it should balance the following trade-off: a low frequency would result in little dissipated power, making difficult to heat the device; opposite, a high frequency could induce dynamic effects (as detailed in Section 3.2) that would compromise the quasi-static tests assumption, needed to be compliant with the modelling approach of the nonlinear block. A 2.5Hz frequency has been eventually chosen. The decrease of the maximum force, as the temperature rises, is clearly visible.

A different perspective on the temperature effect is provided by the force–speed maps in Figure 7. These maps have been obtained firstly letting the damper rest in the thermal chamber until thermal equilibrium and then repeating the very same tests in Figure 4. Due to their limited duration, and the resulting little dissipated energy, the temperature increase during the test is in fact negligible. The experimental

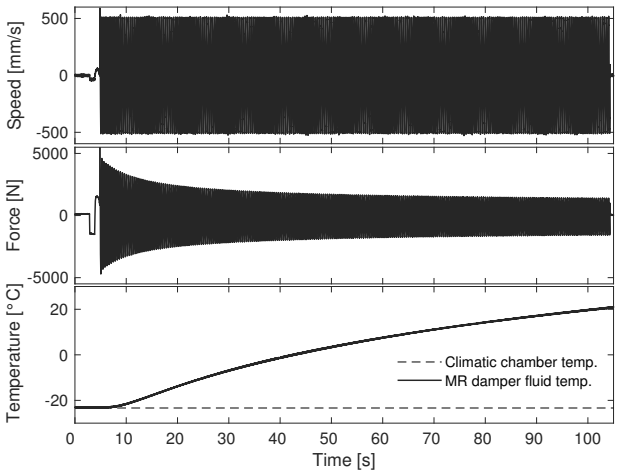

Figure 6: Constant frequency sine wave test for temperature influence investigation.

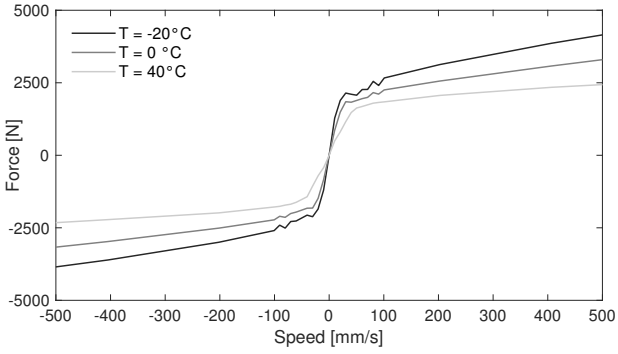

Figure 7: Experimental force–speed nonlinear relationship at different MR fluid temperatures.

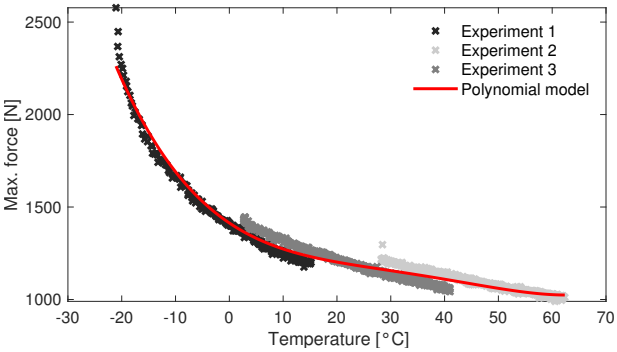

Figure 8: Maximum force dependency from the MR fluid temperature, for the constant frequency sinewave test.

maps show that not only the maximum but the entire damping map is enhanced when the temperature is lower. Thus, from a modelling perspective, the fluid temperature does not affect the shape of the curve, which can still be represented by a piecewise linear function, but it only scales the damping force by a proportional factor, $\alpha(T)$.

$$\hat{F}_c = C(i, \Delta\dot{z})\alpha(T). \tag{3}$$

The dependency of the scaling factor $\alpha(T)$ from the temperature can be retrieved by properly fitting the maximum force *vs* fluid temperature curve, shown in Figure 8 where each point corresponds to one peak of the sine wave. This plot firstly allows one to quantitatively appreciate the relevance of the effect of the temperature on the damper force, which decreases more than 57% within the 80 °C temperature span; the steepest performance loss happens in the coldest conditions. Moreover, it can be seen how the scaling factor $\alpha(T)$ can be effectively modelled with a polynomial function.

3.2. Hysteretic Behaviour

The hysteresis in the force – speed map is a typical feature of MR dampers. Being a dynamic effect, it can be well experimentally emphasized at the test bench using sinusoidal stroke profiles, as those depicted in Figure 9, designed to achieve the same peak speed for different excitation frequencies. To

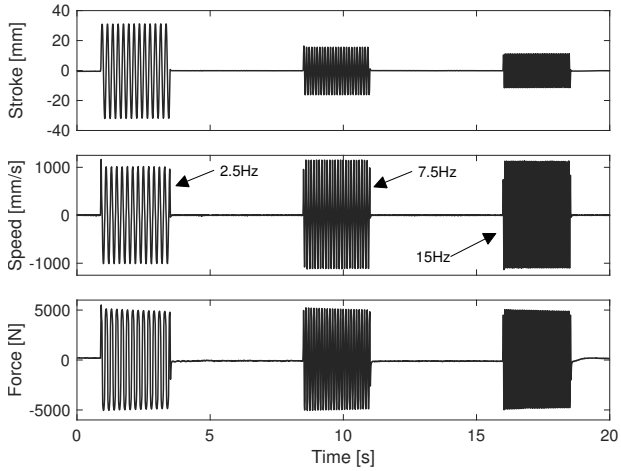

Figure 9: Sinusoidal profiles at different frequency for the identification of the hysteretic behaviour.

mitigate the related temperature increase, the duration of each profile has been limited. The resulting force – speed maps are depicted in Figure 10, where it is possible to observe that the higher the frequency of excitation, the wider the hysteresis in the map. As further confirmation, one should notice how the quasi-static force – speed map lacks any hysteresis.

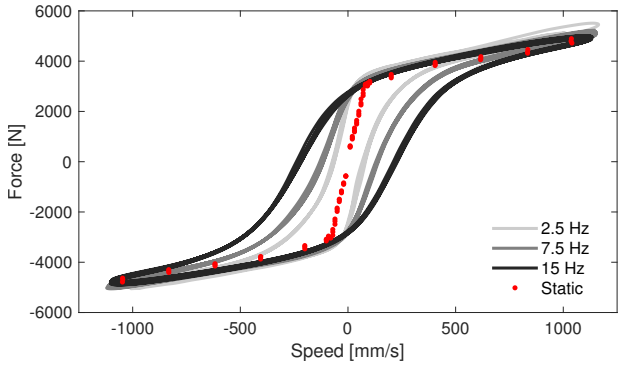

Figure 10: Experimental hysteretic behaviour of the MR damper for different excitation frequencies.

The same sinusoidal test, repeated for different current values and shown in Figure 11, reveals how the hysteresis is not affected by this variable (which affects, as already discussed, only the damping force amplitude). Such evidence validates the modelling

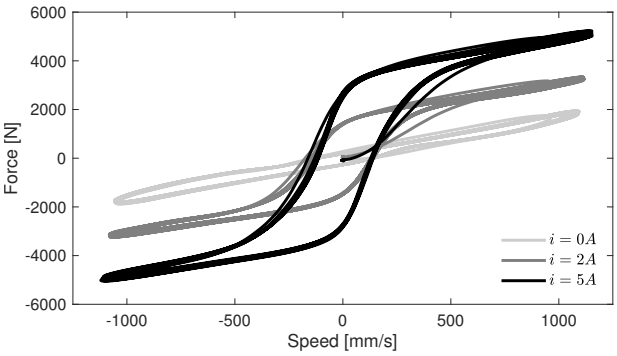

Figure 11: Experimental hysteretic behaviour of the MR damper for different input currents.

scheme proposed in Figure 2 where the hysteretic behaviour is achieved by means of the Hammerstein block $H(s)$.

The identification of the transfer function $H(s)$ is done using the sinusoidal experiments performed at constant current in order to set apart the effects due to the magnetization dynamics. $H(s)$ is identified by minimization of the root mean squared difference between the measured force F and the model output $\hat{F}_h$

$$\|F - \hat{F}_h\|_2 = \|F - H(s)C(i, \Delta\dot{z})\|_2 \qquad (4)$$

where F, i and $\dot{z}$ are the measured force, current and stroke speed profile respectively. The best matching of the experimental data has been obtained with a fourth-order transfer function:

$$H(s) = \frac{p_1 p_2 p_3 p_4}{\omega^2} \frac{s^2 + 2\xi\omega s + \omega^2}{(s+p_1)(s+p_2)(s+p_3)(s+p_4)}. \qquad (5)$$

where the unitary gain has been imposed, considering that the amplitude of the damping force depends by the static block $C(i, \Delta\dot{z})$ of the Hammerstein–Wiener scheme. The resulting parameters are reported in Table 1.

Table 1: Identified parameters for the Hammerstein block.

p_1	p_2	p_3	p_4	ξ	ω
47	111	319	2082	0.97	63

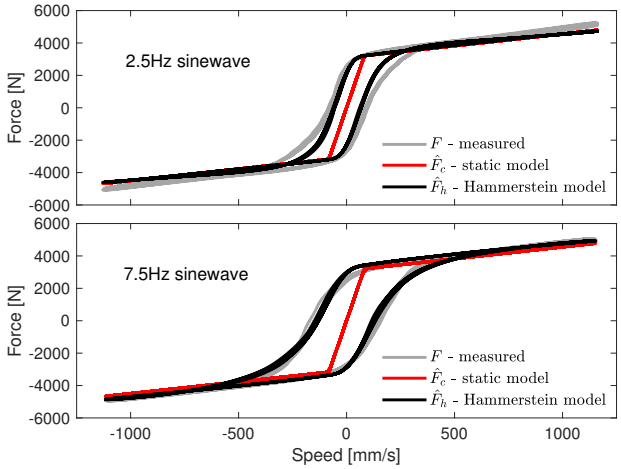

Figure 12: Hysteretic behaviour modelled with the Hammerstein scheme, compared with experimental data and static model at different excitation frequencies.

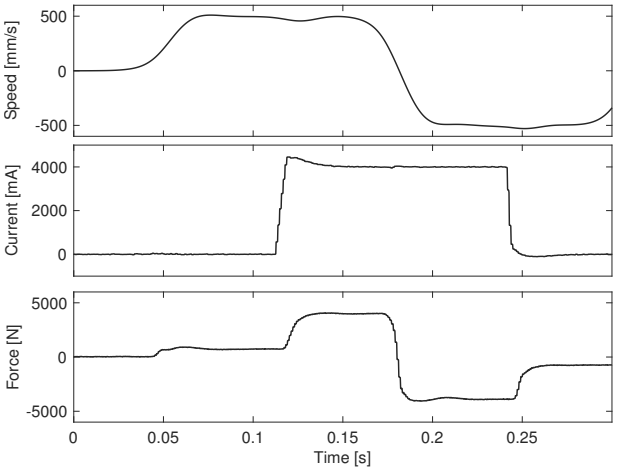

Figure 13: Current step during a constant stroke speed experiment, for the investigation of the magnetization dynamics.

In order to appreciate the identification results, the stroke speed–force map is shown in Figure 12, where three quantities are discriminated:

- F, the force measured by the test bench;
- $\hat{F}_c = C(i, \Delta\dot{z})$, the force solely modelled via the static characteristics;
- $\hat{F}_h = H(s)\hat{F}_c$, the force modelled adding the Hammerstein model part.

This comparison clearly shows the increased accuracy introduced by the Hammerstein block $H(s)$, consistent even when different frequencies are excited.

3.3. Magnetization Dynamics

The viscosity of the MR fluid is controlled via the injected current into the coil of the piston's head which, in turn, modulates the strength of the magnetic field; the iron particles in the fluid align themselves with respect to the field and increase fluid-dynamic friction when flowing through the orifices. In this section, we investigate the time response of this chain of events by designing an *ad hoc* experiment, shown in Figure 13: the current is kept constant to zero and the piston is moved at constant speed; at half way the stroke length, the current is raised. Being the speed constant, as discussed in Section 3.1, the recorded force transients are imputable to the sole magnetization dynamics. In order to model such effects, the Wiener block $M(s)$ is used, introducing the current-to-force dynamics under investigation.

Similarly to $H(s)$, also $M(s)$ is identified by minimizing the root mean squared error between the measured force F and the model output $\hat{F}_{hw}$, that includes also the previously identified block $H(s)$:

$$\|F - \hat{F}_{hw}\|_2 = \|F - H(s)C(M(s)i, \Delta\dot{z})\|_2. \qquad (6)$$

The identified transfer function features a second order dynamics with a delay

$$M(s) = \frac{p_1 p_2}{z} \frac{s+z}{(s+p_1)(s+p_2)} e^{-\tau s}, \qquad (7)$$

and the resulting parameters are reported in Table 2. Also for the Wiener block, the gain of the model has been set equal to one.

Table 2: Identified parameters for the Wiener block.

p_1	p_2	z	τ
124.7	657.5	219.7	0.004

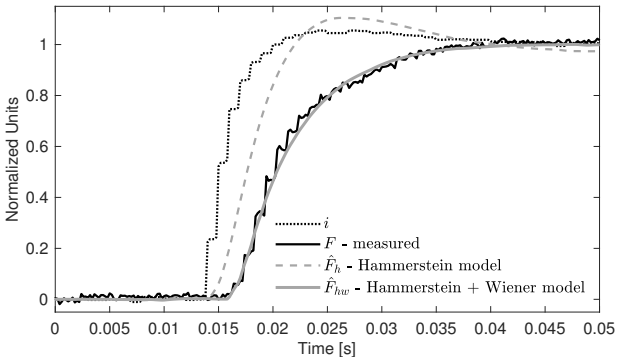

Figure 14: Magnetization dynamics modelling results.

The modelling performance are shown in Figure 14, where the measured force F is compared against the estimated force $\hat{F}_{hw}$. All the quantities are normalized between $[0, 1]$ so that the input current i can also be shown, highlighting the transient. In order to better appreciate the role of the magnetization dynamics, the estimated force $\hat{F}_h$, computed without the Wiener block $M(s)$, is also shown. Similar experiments have been performed using falling current references, to test the system demagnetization response. As a matter of fact, the damper exhibits a symmetrical and consistent behaviour, resulting in no need for any model modifications. For the sake of conciseness, demagnetization experiment plots are omitted.

From a frequency domain perspective, the current-to-force dynamics exhibits a common low-pass filter behaviour with a bandwidth of approximatively 30Hz.

4. Validation

The validation of the overall model, as in Figure 2, is performed with an experiment where the MR damper is excited with a real road solicitation and a Pseudo Random Binary Signal (PRBS) injected as current; the experiment is shown in Figure 15. The PRBS is designed so to have a frequency content within the range 0–20Hz, which is representative of the vehicle vertical dynamics (sprung and unsprung mass) that is meant to be controlled with the damper; moreover, the amplitude of the PRBS signal has been randomly changed at each step, so to span all the possible current values. Notice that this experiment has not been employed in the training of the models and it is therefore a fair validation.

The proposed model is compared against a neural network. The chosen network architecture is a dynamic feed-forward one – as proposed in [22, 23] – which is trained with all the experiments detailed in Section 3; the employed regressors are the stroke speed and the electric current sampled at the present time and at one past instant spaced by $4ms$ in time. In particular, a double hidden layer structure has shown better results with respect to a single layer with the same number of parameters. The numbers of neurons in both hidden layers has been selected in order to reach the best accuracy without overly increasing the number of parameters; the best choice revealed to be 3 neurons for each hidden layer for a total of 31 parameters.

The bar plot in Figure 16 compares the modelling performance of the proposed Hammerstein–Wiener scheme against the Neural Network one, using the root mean squared (RMS) error between the measured and the modelled damper force as quantitative index. It is evident how the complete model is not far from the performance of the Neural Network (less than $50N$ difference) with the advantages of having fewer parameters and a scheme where each block has a semantic correspondence to a physical phenomenon. Furthermore, the proposed model is a control oriented model, more easily integrated the control design process than a Neural Network. The achieved RMS value is close to the declared accuracy of the test bench (approximately $100N$) which proves that the estimation is performing at the limits of the repeatability of the measurement. The bar plot shows also the model accuracy related to the three main characteristics of a MR damper – the static map, the dynamic hysteretic effect and the magnetization dynamics – allowing to assess the relevance of each component. In addition, the percentage error-to-signal ratio (ESR) index, as in [20], is reported; this allows to easily frame the obtained results with the available literature. For instance, [22] well documents and compares different modelling approaches

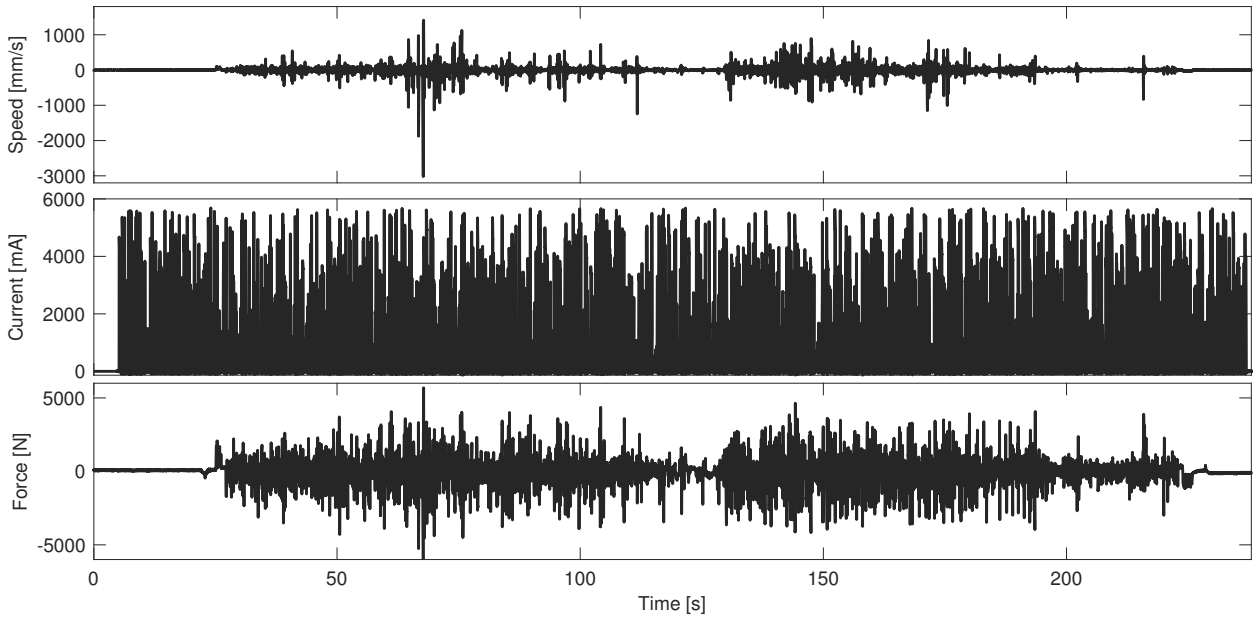

Figure 15: Model validation experiment overview: real road excitation profile and PRBS randomly generated input current.

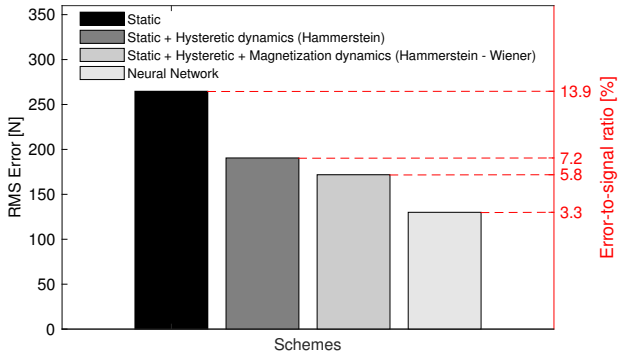

Figure 16: Comparison of the estimation RMS error and percentage error-to-signal ratio (ESR) for different model schemes on the validation test.

using the ESR index and a road profile excitation with PRBS current input. The proposed HW model performance is comparable to the best literature solutions, with an ESR value of 5.8%.

The time domain model results are shown in Figure 17 where only a portion of the experiment is highlighted in order to visually appreciate the estimation accuracy of the proposed Hammerstein–Wiener scheme.

Eventually, in order to emphasize the role of the temperature compensation in the static model, the validation experiment has been repeated at -20 °C, where the temperature effect is particularly significant. The results are shown in Figure 15: in the upper plot the complete model is shown whereas in the bottom one the temperature effect is neglected, mistakenly assuming $T = 25$ °C. The comparison between the two plots clearly reveals the benefits of including the temperature component in the model. The inspection of the second plot reinforces this concept: the modelling error decreases while the temperature increases towards the nominal value.

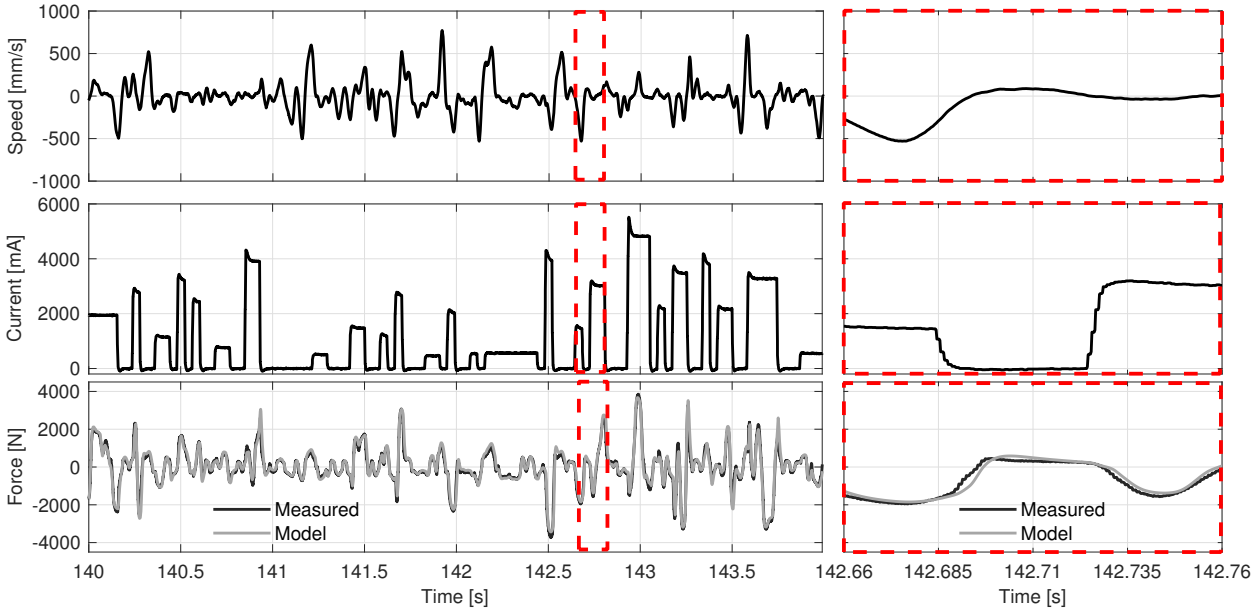

Figure 17: Complete model performance on the validation test.

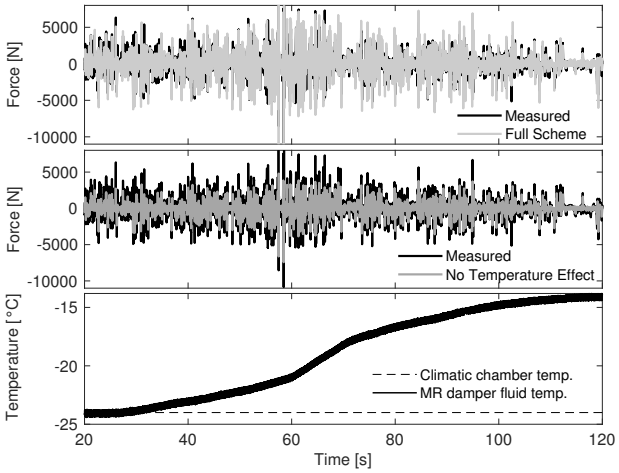

Figure 18: Validation test performed at low temperatures: comparison between the modelling performance of the complete (top plot) scheme and a simplified one (bottom plot) where the temperature effect is neglected.

5. Conclusion

In this article, a control-oriented model for a semi-active MR damper based on a Hammerstein–Wiener scheme is presented. The four main phenomena describing a MR damper (damping characteristics, hysteretic behaviour, magnetization dynamics and temperature effect) are investigated with *ad hoc* experiments and modelled with a specific black-box component. The proposed model is validated on a testbench using a realistic road solicitation, yielding estimation performance close to the one of a Neural Network, with the benefits of a simpler parametrization and a better understanding of the dynamics. In particular, the importance of modelling the magnetization dynamics to improve the estimation performance is shown. The proposed model can be efficiently employed in semi-active magneto-rheological dampers vehicle applications, where the estimation and control strategies can be designed, for instance, profiting by Hammerstein–Wiener techniques.

References

[1] A.-G. Olabi, A. Grunwald, Design and application of magneto-rheological fluid, Materials & design 28 (10) (2007) 2658–2664.

[2] S. Hong, S. Choi, Y. T. Choi, N. M. Wereley, A hydro-mechanical model for hysteretic damping force prediction of er damper: experimental verification, Journal of Sound and Vibration 285 (4-5) (2005) 1180–1188.

[3] N. M. Wereley, L. Pang, Nondimensional analysis of semi-active electrorheological and magnetorheological dampers using approximate parallel plate models, Smart materials and structures 7 (5) (1998) 732.

[4] G. Yang, B. Spencer Jr, J. Carlson, M. Sain, Large-scale mr fluid dampers: modeling and dynamic performance considerations, Engineering structures 24 (3) (2002) 309–323.

[5] A. Sternberg, R. Zemp, J. C. De La Llera, Multiphysics behavior of a magneto-rheological damper and experimental validation, Engineering Structures 69 (2014) 194–205.

[6] D. Wang, W. H. Liao, Magnetorheological fluid dampers: a review of parametric modelling, Smart materials and structures 20 (2) (2011) 023001.

[7] N. D. Sims, N. Holmes, R. Stanway, A unified modelling and model updating procedure for electrorheological and magnetorheological vibration dampers, Smart materials and structures 13 (1) (2003) 100.

[8] İ. Şahin, T. Engin, Ş. Çeşmeci, Comparison of some existing parametric models for magnetorheological fluid dampers, Smart materials and structures 19 (3) (2010) 035012.

[9] B. F. Spencer, S. J. Dyke, M. K. Sain, J. D. Carlson, Phenomenological model for magnetorheological dampers, Journal of Engineering Mechanics 123 (3) (1997) 230–238. doi:10.1061/(ASCE)0733-9399(1997)123:3(230).

[10] A. Dominguez, R. Sedaghati, I. Stiharu, Modelling the hysteresis phenomenon of magnetorheological dampers, Smart Materials and Structures 13 (6) (2004) 1351.

[11] Q. Zhou, S. Nielsen, W. Qu, Semi-active control of three-dimensional vibrations of an inclined sag cable with magnetorheological dampers, Journal of Sound and Vibration 296 (1) (2006) 1 – 22.

[12] R. Jiménez, L. Álvarez-Icaza, Lugre friction model for a magnetorheological damper, Structural Control and Health Monitoring 12 (1) (2005) 91–116.

[13] J. Kasprzyk, J. Wyrwał, P. Krauze, Automotive mr damper modeling for semi-active vibration control, in: 2014 IEEE/ASME International Conference on Advanced Intelligent Mechatronics, IEEE, 2014, pp. 500–505.

[14] G. Hu, Q. Liu, R. Ding, G. Li, Vibration control of semi-active suspension system with magnetorheological damper based on hyperbolic tangent model, Advances in Mechanical Engineering 9 (5) (2017) 1687814017694581.

[15] M. Braz-César, R. Barros, Numerical modeling of magneto-rheological dampers, Mecânica Experimental 22 (2013) 147–159.

[16] F. Weber, Bouc–wen model-based real-time force tracking scheme for mr dampers, Smart Materials and Structures 22 (4) (2013) 045012.

[17] S.-B. Choi, S.-K. Lee, Y.-P. Park, A hysteresis model for the field-dependent damping force of a magnetorheological damper, Journal of sound and vibration 245 (2) (2001) 375–383.

[18] V. Atray, P. Roschke, Design, fabrication, testing, and fuzzy modeling of a large magnetorheological damper for vibration control in a railcar, Proceedings of the 2003 IEEE/ASME Joint Railroad Conference (2003) 223 – 229.

[19] D. Truong, K. Ahn, Mr fluid damper and its application to force sensorless damping control

system, Smart Actuation and Sensing Systems-Recent Advances and Future Challenges, In-Tech, Rijeka (2012) 383–424.

[20] S. M. Savaresi, S. Bittanti, M. Montiglio, Identification of semi-physical and black-box nonlinear models: the case of mr-dampers for vehicles control, Automatica 41 (1) (2005) 113–127.

[21] Y. He, G. Liang, B. Xue, Z. Peng, Y. Wei, A unified mr damper model and its inverse characteristics investigation based on the neuro-fuzzy technique, International Journal of Applied Electromagnetics and Mechanics 61 (2) (2019) 225–245.

[22] J. Tudón-Martínez, J. d. J. Lozoya-Santos, R. Morales-Menendez, R. Ramirez-Mendoza, An experimental artificial-neural-network-based modeling of magneto-rheological fluid dampers, Smart Materials and Structures 21 (8) (2012) 085007.

[23] M. Khalid, R. Yusof, M. Joshani, H. Selamat, M. Joshani, Nonlinear identification of a magneto-rheological damper based on dynamic neural networks, Computer-Aided Civil and Infrastructure Engineering 29 (3) (2014) 221–233.

[24] Q. Liu, W. Chen, H. Hu, Q. Zhu, Z. Xie, An optimal narx neural network identification model for a magnetorheological damper with force-distortion behavior, Frontiers in Materials 7 (2020) 10.

[25] C. A. Duchanoy, M. A. Moreno-Armendáriz, J. C. Moreno-Torres, C. A. Cruz-Villar, A deep neural network based model for a kind of magnetorheological dampers, Sensors 19 (6) (2019) 1333.

[26] M. Cheng, X. Jiao, Modified active disturbance rejection control for non-linear semi-active vehicle suspension with magneto-rheological damper, Transactions of the Institute of Measurement and Control 40 (8) (2018) 2611–2621.

[27] A. O. Bashir, X. Rui, J. Zhang, Ride comfort improvement of a semi-active vehicle suspension based on hybrid fuzzy and fuzzy-pid controller, Stud. Inform. Control 28 (2019) 421–430.

[28] X. Du, G. Han, M. Yu, Y. Peng, X. Xu, J. Fu, Fault detection and fault tolerant control of vehicle semi-active suspension system with magneto-rheological damper, Smart Materials and Structures 30 (1) (2020) 014004.

[29] F. Weber, H. Distl, Amplitude and frequency independent cable damping of sutong bridge and russky bridge by magnetorheological dampers, Structural Control and Health Monitoring 22 (2) (2015) 237–254.

[30] V. N. Mai, D.-S. Yoon, S.-B. Choi, G.-W. Kim, Explicit model predictive control of semi-active suspension systems with magneto-rheological dampers subject to input constraints, Journal of Intelligent Material Systems and Structures 31 (9) (2020) 1157–1170.

[31] D. X. Phu, J.-H. An, S.-B. Choi, et al., A novel adaptive pid controller with application to vibration control of a semi-active vehicle seat suspension, Applied Sciences 7 (10) (2017) 1055.

[32] J. Yu, X. Dong, Z. Zhang, A novel model of magnetorheological damper with hysteresis division, Smart Materials and Structures 26 (10) (2017) 105042.

[33] J. Yu, X. Dong, X. Wang, C. Pan, Y. Zhou, Asymmetric dynamic model of temperature-dependent magnetorheological damper and application for semi-active system, Frontiers in Materials 6 (2019) 227.

[34] H. Deng, R. Yue, X. Lian, J. Deng, J. Zhang, M. Ma, X. Zhong, Self-updating inverse model for magnetorheological dampers, Smart Materials and Structures 28 (11) (2019) 115033.

[35] M. Cheng, Z. Chen, W. Liu, Y. Jiao, A novel parametric model for magnetorheological dampers considering excitation characteristics, Smart Materials and Structures 29 (4) (2020) 045002.

[36] D. Wang, W. Liao, Modeling and control of magnetorheological fluid dampers using neural networks, Smart materials and structures 14 (1) (2004) 111.

[37] X.-M. Du, M. Yu, J. Fu, Y.-X. Peng, H.-F. Shi, H. Zhang, H_∞ control for a semi-active scissors linkage seat suspension with magnetorheological damper, Journal of Intelligent Material Systems and Structures 30 (5) (2019) 708–721.

[38] A. S. Gad, W. Oraby, H. Metered, Vibration control of semi-active vehicle suspension system incorporating mr damper using fuzzy self-tuning pid approach, Tech. rep., SAE Technical Paper (2020).

[39] A.-A. Zamani, S. Tavakoli, S. Etedali, J. Sadeghi, Adaptive fractional order fuzzy proportional–integral–derivative control of smart base-isolated structures equipped with magnetorheological dampers, Journal of Intelligent Material Systems and Structures 29 (5) (2018) 830–844.

[40] F. Oliveira, M. A. Botto, P. Morais, A. Suleman, Semi-active structural vibration control of base-isolated buildings using magnetorheological dampers, Journal of Low Frequency Noise, Vibration and Active Control 37 (3) (2018) 565–576.

[41] J. C. Tudon-Martinez, D. Hernandez-Alcantara, L. Amezquita-Brooks, R. Morales-Menendez, J. de J Lozoya-Santos, O. Aquines, Magnetorheological dampers model influence on the semi-active suspension performance, Smart Materials and Structures 28 (10) (2019) 105030.

[42] X. Tang, H. Du, S. Sun, D. Ning, Z. Xing, W. Li, Takagi–sugeno fuzzy control for semi-active vehicle suspension with a magnetorheological damper and experimental validation, IEEE/ASME transactions on mechatronics 22 (1) (2016) 291–300.

[43] D.-S. Yoon, G.-W. Kim, S.-B. Choi, Response time of magnetorheological dampers to current inputs in a semi-active suspension system: Modeling, control and sensitivity analysis, Mechanical Systems and Signal Processing 146 (2021) 106999.

[44] R. Jeyasenthil, S. Choi, A novel semi-active control strategy based on the quantitative feedback theory for a vehicle suspension system with magneto-rheological damper saturation, Mechatronics 54 (2018) 36–51.

[45] X. Wang, Semi-active adaptive optimal control of vehicle suspension with a magnetorheological damper based on policy iteration, Journal of Intelligent Material Systems and Structures 29 (2) (2018) 255–264.

[46] X. Song, M. Ahmadian, S. Southward, L. Miller, An adaptive semiactive control algorithm for magnetorheological suspension systems, Journal of Vibration and Acoustics, Transactions of the ASME 127 (5) (2005) 493–502. doi:10.1115/1.2013295.

[47] X. Song, M. Ahmadian, S. C. Southward, Modeling magnetorheological dampers with application of nonparametric approach, Journal of intelligent material systems and structures 16 (5) (2005) 421–432.

[48] K. El Majdoub, D. Ghani, F. Giri, F. Chaoui, Adaptive semi-active suspension of quarter-vehicle with magnetorheological damper, Journal of Dynamic Systems, Measurement, and Control 137 (2) (2015).

[49] J. de Jesus Lozoya-Santos, O. Sename, L. Dugard, R. Morales-Menéndez, R. Ramirez-Mendoza, A semi-active control-oriented damper model for an automotive suspension, IFAC Proceedings Volumes 43 (7) (2010) 336–341.

[50] J. de Jesus Lozoya-Santos, O. Sename, L. Dugard, R. Morales-Menéndez, R. Ramirez-Mendoza, A lpv quarter of car with semi-active suspension model including dynamic input saturation, IFAC Proceedings Volumes 43 (21) (2010) 68–75.

[51] M. M. Morato, O. Sename, L. Dugard, M. Q. Nguyen, Fault estimation for automotive electrorheological dampers: Lpv-based observer approach, Control Engineering Practice 85 (2019) 11–22.

[52] M. M. Morato, T.-P. Pham, O. Sename, L. Dugard, Development of a simple er damper model for fault-tolerant control design, Journal of the Brazilian Society of Mechanical Sciences and Engineering 42 (10) (2020) 1–22.

[53] A. Wills, T. B. Schön, L. Ljung, B. Ninness, Identification of hammerstein–wiener models, Automatica 49 (1) (2013) 70–81.

[54] H. Bloemen, T. Van Den Boom, H. Verbruggen, Model-based predictive control for hammerstein-wiener systems, International Journal of Control 74 (5) (2001) 482–495.

[55] F. Khani, M. Haeri, Robust model predictive control of nonlinear processes represented by wiener or hammerstein models, Chemical Engineering Science 129 (2015) 223–231.

[56] B. Zhang, H. Hong, Z. Mao, Adaptive control of hammerstein–wiener nonlinear systems, International Journal of Systems Science 47 (9) (2016) 2032–2047.

[57] J. Wang, A. Sano, T. Chen, B. Huang, Blind hammerstein identification for mr damper modeling, in: 2007 American Control Conference, IEEE, 2007, pp. 2277–2282.

[58] J. Wang, A. Sano, T. Chen, B. Huang, Identification of hammerstein systems without explicit parameterisation of non-linearity, International Journal of Control 82 (5) (2009) 937–952.

[59] G. Jin, M. K. Sain, B. F. Spencer, Modeling mr-dampers: the ridgenet estimation approach, in: Proceedings of the 2002 American Control Conference (IEEE Cat. No. CH37301), Vol. 3, IEEE, 2002, pp. 2457–2462.

[60] G. Jin, M. K. Sain, B. Spencer, Nonlinear blackbox modeling of mr-dampers for civil structural control, IEEE Transactions on Control Systems Technology 13 (3) (2005) 345–355.

[61] S. Kanarachos, D. Savitski, N. Lagaros, M. E. Fitzpatrick, Automotive magnetorheological dampers: modelling and parameter identification using contrast-based fruit fly optimisation, Soft Computing 22 (24) (2018) 8131–8149.

[62] J. Lozoya-Santos, R. Morales-Menendez, R. Ramirez-Mendoza, Design of experiments for mr damper modelling, in: 2009 International Joint Conference on Neural Networks, IEEE, 2009, pp. 1915–1922.

[63] J. de J Lozoya-Santos, R. Morales-Menendez, R. Ramirez-Mendoza, J. C. Tudón-Martinez, O. Sename, L. Dugard, Magnetorheological damper—an experimental study, Journal of Intelligent Material Systems and Structures 23 (11) (2012) 1213–1232.

[64] M. J. McKee, Effects of temperature on performance of compressible magnetorheological fluid dampers, University of Nevada, Reno, 2010.